Acta Materialia 206 (2021) 116611

Contents lists available at ScienceDirect

Acta Materialia

journal homepage: www.elsevier.com/locate/actamat

The role of grain colony on secondary recrystallization in grain-oriented electrical steel: New insights from an original tracking experiment

Hong-Yu Song[a,*], Yin-Ping Wang[a], Claude Esling[b,c], Guo-Dong Wang[a], Hai-Tao Liu[a,**]

[a] State Key Laboratory of Rolling and Automation, Northeastern University, Shenyang 110819, PR China
[b] Université de Lorraine, CNRS, Arts et Métiers ParisTech, LEM3, F-57000 Metz, France
[c] Laboratory of Excellence on Design of Alloy Metals for low-mAss Structures (DAMAS), Université de Lorraine, F-57070, Metz, France

ARTICLE INFO

Article history:
Received 10 August 2020
Revised 29 November 2020
Accepted 26 December 2020
Available online 30 December 2020

Keywords:
Microstructure
Texture
Abnormal grain growth
Recrystallization
Grain colony

ABSTRACT

Secondary recrystallization is responsible for the sharp Goss texture ({110}<001>) of grain-oriented electrical steels. Many investigations have focused on establishing the relations between the sharpness of final Goss textures and primary recrystallization textures measured by the X-ray diffraction. However, the contributions of micro-texture characteristics to secondary recrystallization have not yet been well understood. Here, we report that the grain colonies composed of grains with similar orientations in the primary recrystallization matrix had a particular role on the development of secondary recrystallization via an original tracking experiment. We observe that the γ-grain (<111>//normal direction, ND) colonies facilitate the retention of primary recrystallization matrix grains ($\leq$25μm) having 20-45° disorientation with {110}<001> and relatively large difference in the associated frequency with precise Goss orientation and that having deviation angle of 15°, promoting the abnormal growth of low-deviation-angle Goss grains especially after the onset of secondary recrystallization and leading to sharp final Goss texture. By contrast, the abnormal growth of high-deviation-angle Goss grains may be also promoted after the initiation of secondary recrystallization in case of randomly-distributed γ-grains in primary recrystallization matrix and thus resulted in deteriorated magnetic properties. In this way, we reveal the role of grain colony on secondary recrystallization and the underlying mechanism for the effect of primary recrystallization textures on the sharpness of final Goss texture. We also observe that the formation of grain colonies is mainly related to the initial solidification microstructure, processing route as well as the deformation and recrystallization features of γ-grains.

1. Introduction

Texture control intends to take advantage of the anisotropies of physical and mechanical properties of the materials by promoting the development of desired crystallographic orientations [1-5]. For the grain-oriented electrical steels which are mainly used as the core material of transformers, a sharp Goss texture is expected because it ensures that the easiest magnetization directions (<100>) of grains are parallel to the rolling direction (RD) [1,6,7]. Dunn [8,9] first, followed by others [10-12] demonstrated that this sharp Goss texture is generated by secondary recrystallization during high temperature annealing in which a small portion of Goss grains embodied in the primary recrystallization matrix grow abnormally. In order to improve the magnetic properties by sharpening the final Goss texture, different mechanisms have been proposed to understand the secondary recrystallization process, i.e., grain size advantage theory [13,14], coincidence site lattice grain boundary theory [15-17], high energy grain boundary theory [18-20], low surface energy theory [21,22], solid state wetting theory [23-25], dislocation-related stored energy theory [26-28] and so on. Recently, Birosca et al. [29] reported the significant influences of the external heat flux direction on the abnormal growth of Goss grains, which provided a new viewpoint on understanding the development of secondary recrystallization. However, there are still arguments because none of them can completely explain the secondary recrystallization process, especially the sharpness of final Goss texture.

Many investigations focused on establishing the relations between the sharpness of final Goss textures and primary recrys-

* Corresponding author.
** Corresponding author.
E-mail addresses: sohoyu@126.com (H.-Y. Song), liuht@ral.neu.edu.cn, liu_haitao163@163.com (H.-T. Liu).

https://doi.org/10.1016/j.actamat.2020.116611
1359-6454/

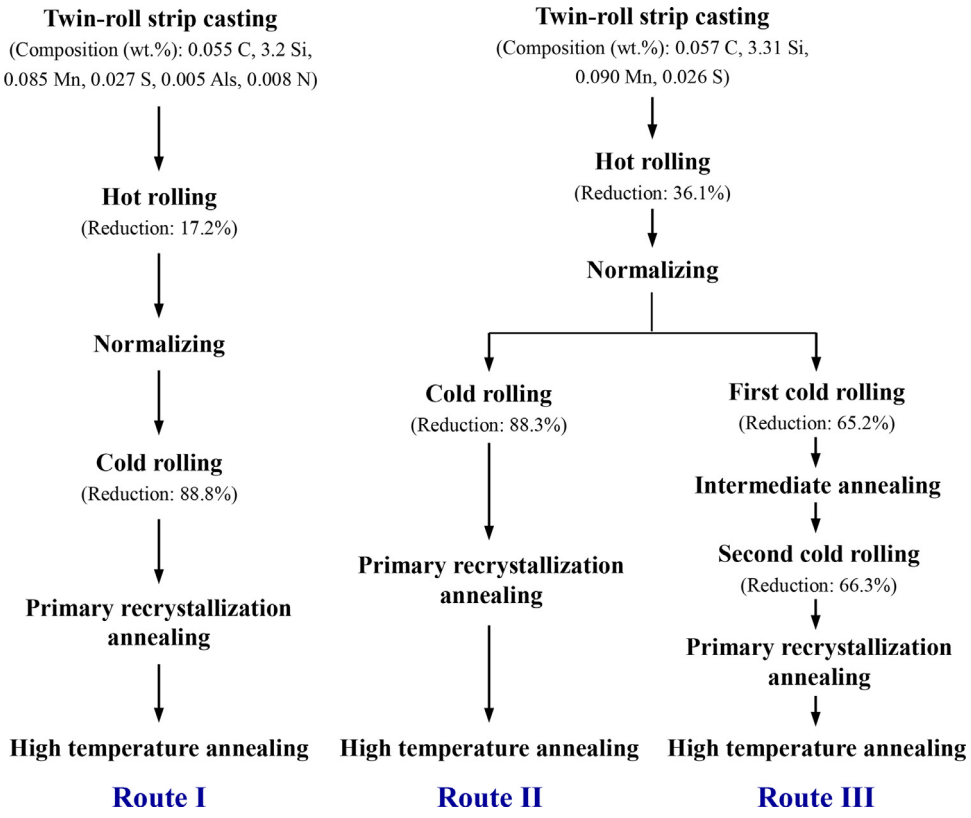

Fig. 1. Schematic diagram showing the experimental procedures in various routes.

tallization textures measured by X-ray diffraction [30-32]. It is reported that the primary recrystallization textures of the high-permeability and conventional grain-oriented electrical steels are normally characterized by a pronounced {111}<112> texture and a uniform γ-fiber texture (<111>//ND), respectively [1,33]. However, these primary recrystallization textures may not represent the actual environments for the initiation of secondary recrystallization because they may still change with increasing temperature [34,35]. Besides, the unconsumed matrix after the onset of secondary recrystallization may also exert significant influences on the abnormal growth of Goss grains. Unfortunately, it is a challenge to accurately examine the orientations of these unconsumed matrix grains after the onset of secondary recrystallization by X-ray diffraction. The Electron Backscatter Diffraction (EBSD) provides an opportunity to investigate the micro-texture evolution [36-38] during the processing route even after the initiation of secondary recrystallization. This may offer more information for understanding the abnormal growth of Goss grains. However, the contributions of micro-texture characteristics to the secondary recrystallization have not yet been well understood.

In the present paper, two kinds of grain-oriented electrical steels were processed with three different routes and an original tracking experiment was carried out to investigate the role of grain colony in the primary recrystallization matrix on secondary recrystallization. Thus, main attention was paid to analyzing the microstructure and micro-texture evolution during primary recrystallization and high temperature annealing. This work led to better understanding of the development of secondary recrystallization.

2. Experimental procedures

2.1. Specimen preparation

A 2.9 mm-thick as-cast strip of grain-oriented electrical steel with the composition (wt%) of 0.055 C, 3.2 Si, 0.085 Mn, 0.027 S, 0.005 Al, 0.008 N and balance Fe was prepared by twin-roll strip casting, as described in detail in previous investigations [39,40]. During the twin-roll strip casting, a low melt superheat was employed to produce a fine solidification microstructure with an average grain size of 45 μm. The as-cast strip was then hot rolled to 2.4 mm-thick (17.2%) at 1130°C and quenched in cold water. The hot rolled sheet was subjected to the normalizing in which the sheet was respectively soaked at 1130°C and 930°C for 2 minutes and quenched in boiling water. The normalized sheets were cold rolled to 0.27 mm (88.8%) and primary recrystallization annealed at 830°C for 5 minutes in a wet atmosphere of 75% (volume fractions) H_2 and 25% N_2. Finally, during the high temperature annealing, the primary recrystallization annealed sheets were heated to 1200°C from 800°C at a heating rate of 15°C/h in a dry atmosphere of 75% H_2 and 25% N_2 and then held at 1200°C for 20h in 100% H_2. For convenience, this processing route was defined as Route I and the schematic diagram was shown in Fig. 1.

By contrast, a high melt superheat was employed to prepare a 3.6 mm-thick as-cast strip with coarse solidification microstructure with an average grain size of 152 μm. The composition (wt%) of this strip was 0.057 C, 3.31 Si, 0.090 Mn, 0.026 S and balance Fe. This as-cast strip was hot rolled to a thickness of 2.3 mm (36.1%) at 1130°C and quenched in cold water. The hot rolled sheets were then subjected to the normalizing in which they were respectively held at 1130°C and 930°C for 2 minutes and quenched in boiling water. Here, two different routes, i.e., Route II and Route III were employed (Fig. 1). For Route II, the normalized sheet was directly cold rolled to 0.27 mm (88.3%). For Route III, the normalized sheet was first cold rolled to 0.8 mm (65.2%), intermediate annealed at 830°C for 5 minutes and finally cold rolled to 0.27 mm (66.3%). The cold rolled sheets in Route II and Route III were subjected to the same primary recrystallization annealing and high temperature annealing as those in Route I.

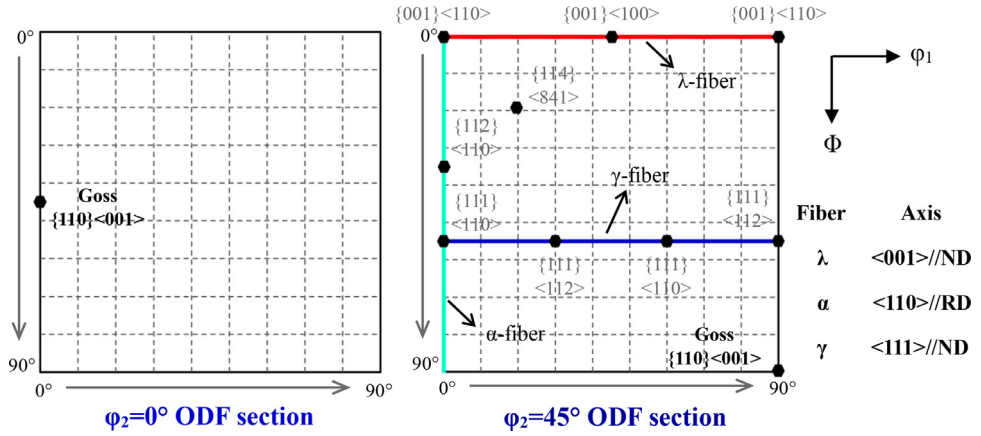

Fig. 2. Typical texture components and definition of fiber textures on φ_2=0° and φ_2=45° ODF sections in grain-oriented electrical steels.

2.2. Tracking experiment

To investigate the microstructure and texture evolution during the processing, an original tracking experiment was carried out. In this experiment, 25 samples with the size of 110 mm (width) × 25 mm (length) were sectioned along the rolling direction of the cold rolled sheet in Route II by wire-electrode cutting. Except the first sample, three adjacent samples (position in the rolling direction) were categorized as one group. In each group, the first sample was selected as the cold rolled sample, while the second and the third one were subjected to the same primary recrystallization annealing in Route II. Then, the third one was subjected to the same high temperature annealing in Route II.

To investigate the microstructure evolution prior to and after the onset of secondary recrystallization, the primary recrystallization annealed samples from Route I, Route III and the tracking experiment in Route II were subjected to an isothermal annealing at 975°C for various times (30 and 45 minutes). Several primary recrystallization annealed samples from the tracking experiment in Route II were annealed at 1000°C for different times (30, 45 and 60 minutes).

2.3. Examination of microstructure, texture and magnetic property

The microstructures were examined using an Olympus optical microscope after grinding, polishing and etching with 4% nital. As for the high temperature annealed sample, a digital camera was used to observe the microstructures on the RD-transverse direction (TD) sections after etching with 10% hydrochloric acid. The Bruker D8 Discover X-ray diffractometer was used to measure three incomplete pole figures of {110}, {200} and {211} in the range of the polar angle α from 0° to 70° with $Co_{K\alpha 1}$ radiation. Then, the Orientation Distribution Functions (ODFs) were calculated from these pole figures by the series expansion method (l_{max}=22) developed by Bunge [41,42]. In this work, the φ_2=0° and φ_2=45° ODF sections were used to reveal the typical texture components in the grain-oriented electrical steels, see Fig. 2. For the EBSD measurements, the samples were ground, polished and electropolished with a 14% perchloric acid/alcohol solution. The EBSD detecting system was equipped in a Zeiss Ultra 55 field emission scanning electron microscope. A variety of step sizes were employed during the EBSD mapping, depending on different grain sizes and investigation purposes. The HKL Channel 5 software (Oxford Instruments) was used to analyze the microstructure and micro-texture characteristics of the samples. The LINKJOIN MATS-2010M tester was employed to measure the magnetic inductions at 800A/m (B_8) of the high temperature annealed sheets. The tester contained a magnetic measurement instrument based on a data acquisition unit with an adapted software package for data analysis. The sample used for measuring magnetic properties was 100 mm along the rolling direction and 30 mm along the transverse direction.

3. Results and discussion

3.1. Correlation between primary recrystallization microstructure and texture and high temperature annealed microstructure, texture and magnetic property

The microstructures and textures obtained after the primary recrystallization annealing are shown in Fig. 3. For Route I, a fine microstructure with an average grain size of 10.2 μm and a strong {111}<112> texture (Fig. 3(a) and Fig. 3(b)) were generated, which were similar to the typical primary recrystallization microstructure and texture by one-stage cold rolling route [1,33,43,44]. For Route II, a homogeneous microstructure together with the medium {111}<112> texture and the λ-fiber texture were produced, see Fig. 3(c) and Fig. 3(d). For Route III, the primary recrystallization annealed sheet had a homogeneous microstructure with an average grain size of 12.4 μm (Fig. 3(e)). In contrast to Route I and Route II, the primary recrystallization texture obtained from Route III was characterized by a medium and uniform γ-fiber texture instead of {111}<112> texture.

After the high temperature annealing, a well-developed secondary recrystallization microstructure composed of coarse Goss grains and a sharp Goss texture were produced from Route I, see Fig. 4(a) and Fig. 4(b). As a result, the magnetic induction B_8 of the high temperature annealed sheet was as high as 1.94 T which was equivalent to that of high-permeability grain-oriented electrical steels produced by conventional routes [1,33]. For Route II, the high temperature annealed sheets had inhomogeneous microstructures comprised of large Goss grains and fine equiaxed grains (Fig. 4(c)). For convenience, the large Goss grain region and fine equiaxed grain region were denoted secondary recrystallization region (outlined by yellow dashed line) and non-secondary recrystallization region, respectively. As shown in Fig. 4(d), the secondary recrystallization region exhibited a sharp Goss texture and a high magnetic induction B_8 of 1.92 T. Nevertheless, most grains in the non-secondary recrystallization regions had various orientations (Fig. 4(e)) and the associated texture was characterized by medium λ-fiber texture and γ-fiber texture components as well as deviated Goss texture (Fig. 4(f)), leading to a magnetic induction B_8 as low as 1.57 T. For Route III, a well-developed secondary recrystallization microstructure composed of large Goss grains was also formed in the high temperature annealed sheet (Fig. 4(g)). How-

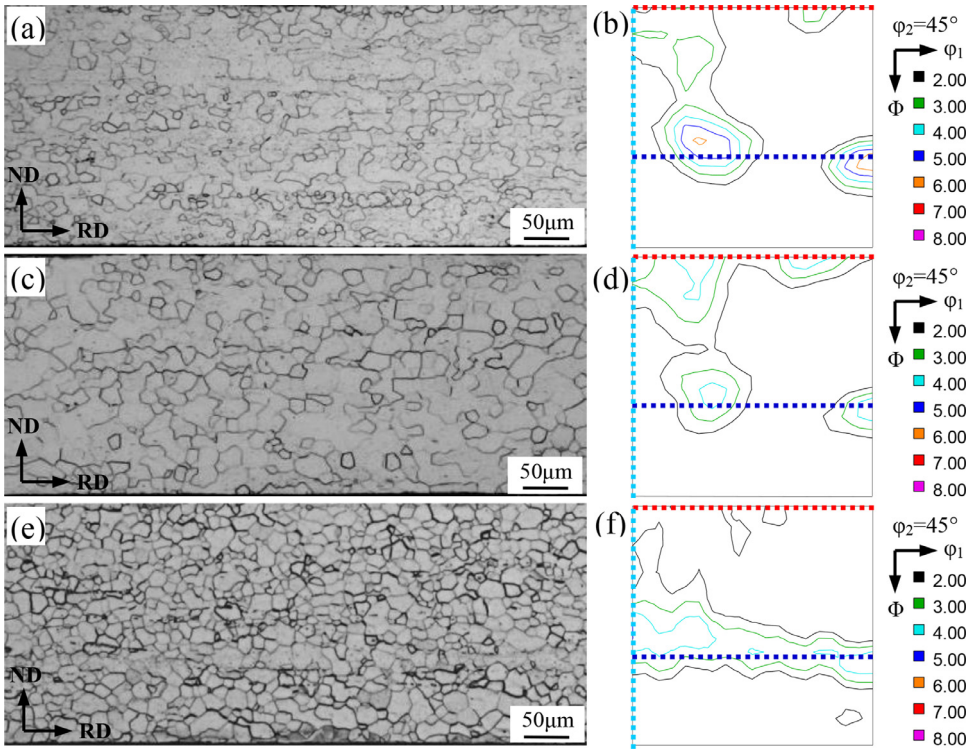

Fig. 3. Primary recrystallization (a) microstructure and (b) texture (φ_2=45° section) in Route I; primary recrystallization (c) microstructure and (d) texture (φ_2=45° section) in Route II; primary recrystallization (e) microstructure and (f) texture (φ_2=45° section) in Route III.

ever, the B_8 value was only 1.86 T which was much lower than that in Route I and that of secondary recrystallization region in Route II due to the relatively weak Goss texture in Fig. 4(h).

The distinct high temperature annealed microstructures, textures and magnetic properties in Fig. 4 suggested that the corresponding primary recrystallization matrices provided various environments for the abnormal growth of Goss grains. Given the homogeneous microstructures in Route I and Route III (Fig. 3 and Fig. 4), it was convenient to track the microstructure and texture evolution along the processing route. By contrast, it was a great challenge to do this in Route II due to the inhomogeneous high temperature annealed microstructure (Fig. 4(c)). Thus, an original tracking experiment (the details were shown in the experimental procedures) was carried out in Route II. The RD-position resolved microstructures (RD-TD section) of the high temperature annealed samples in the tracking experiment are shown in Fig. 5. Surprisingly, although the high temperature annealed samples were separated by the cold rolled sample and primary recrystallization annealed sample (total distance: 50 mm), the secondary recrystallization regions in these samples demonstrated continuous features along the rolling direction, as outlined with the blue frames. This provided an opportunity to investigate the microstructure and texture evolution associated with the secondary recrystallization regions and non-secondary recrystallization regions in the high temperature annealed sheets.

3.2. Environments for abnormal growth of Goss grains in various routes

The sharp final Goss textures in Route I, Route II (secondary recrystallization regions) and Route III (Fig. 4) indicated that their primary recrystallization matrices provided favorable environments for the abnormal growth of Goss grains. Many theories have been proposed to describe these environments [29]. In the high energy theory [18-20], it is thought that the presence of higher frequency of 20-45° boundaries around Goss grains in the primary recrystallization matrix facilitates the abnormal growth of Goss grains. However, as pointed out in many investigations [21,22,29], the frequency of 20-45° boundaries derived from the grain boundary length or ODFs in the primary recrystallization annealed sheet cannot explain the sharpness of final Goss texture. As shown in Fig. 4(a) and Fig. 6, the high temperature annealed sheet in Route III had the weakest final Goss texture and lowest magnetic induction although its primary recrystallization matrix had the highest difference (20.47%) in the frequency of 20-45° boundaries around Goss grains and that of whole matrix.

Unlike the methods proposed in [18-20], in this work, the Euler angles of all the matrix grains were extracted to calculate their disorientation with Goss orientation ({110}<001>). As shown in Fig. 7, the frequencies of grains (≤ 25 μm) having 20-45° disorientation with precise Goss orientation ({110}<001>) were quite similar in the primary recrystallization matrices in the three routes in spite of their distinct microstructures and textures (Fig. 3). For Route I and Route II, the frequencies remained at the relatively high levels even after the onset of secondary recrystallization. As shown, the corresponding frequencies in the unconsumed matrices were still as high as 65.56% and 67.78% in Route I and Route II (Fig. 7), respectively. These two matrices also had large differences (~9%) in the associated frequencies with precise Goss orientation and that having deviation angle of 15°, see Fig. 8. Thus, the abnormal growth of low-deviation-angle Goss grains was still facilitated after the initiation of secondary recrystallization, producing sharp final Goss textures and high magnetic induction (Fig. 4(b) and Fig. 4(d)).

By contrast, for Route III, the frequencies of grains (≤ 25 μm) having 20-45° disorientation with precise Goss orientation was remained at a relatively high value of 61.52% prior to the onset of secondary recrystallization. However, after the onset of secondary recrystallization, it was greatly reduced to 40.80%, see Fig. 7. In addition, the difference in the associated frequencies with pre-

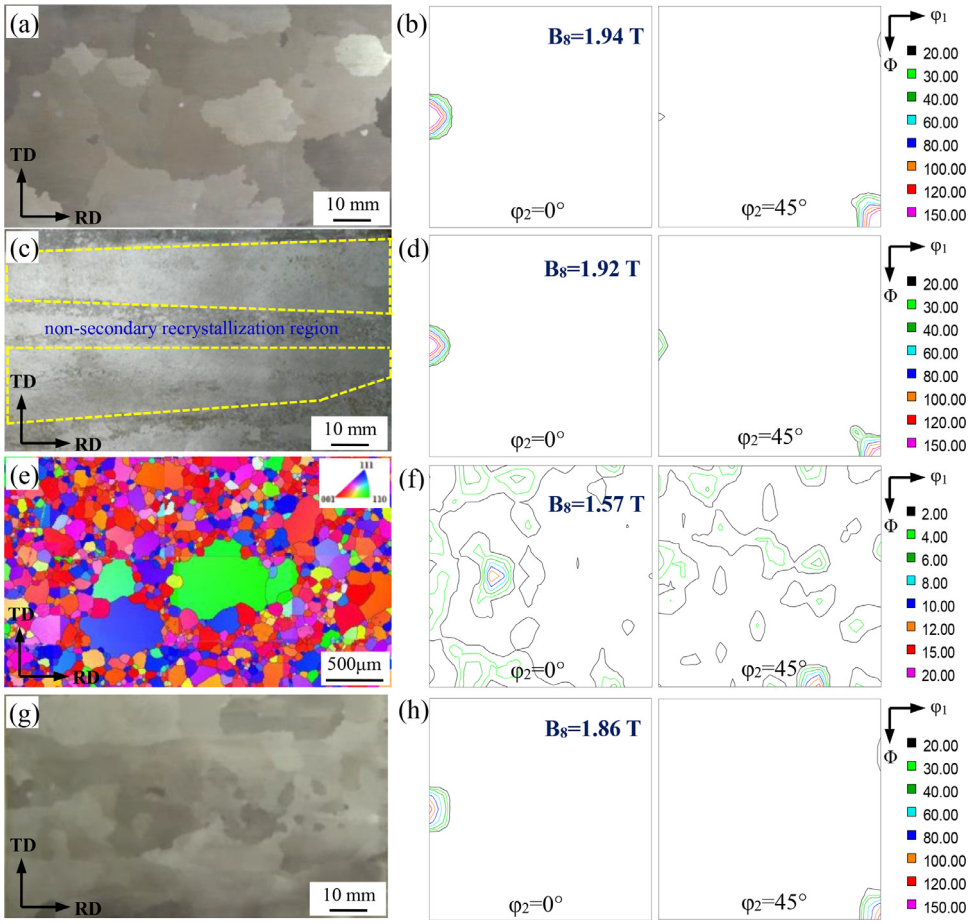

Fig. 4. (a) Microstructure and (b) texture (φ_2=0° and φ_2=45° section) of the high temperature annealed sheet from Route I; (c) microstructure and (d) texture (φ_2=0° and φ_2=45° section) of the secondary recrystallization region of the high temperature annealed sheet from Route II; (e) ND inverse pole figure (IPF) map and (f) texture (φ_2=0° and φ_2=45° section) of the non-secondary recrystallization region of the high temperature annealed sheet from Route II; (g) microstructure and (h) texture (φ_2=0° and φ_2=45° section) of the high temperature annealed sheet from Route III.

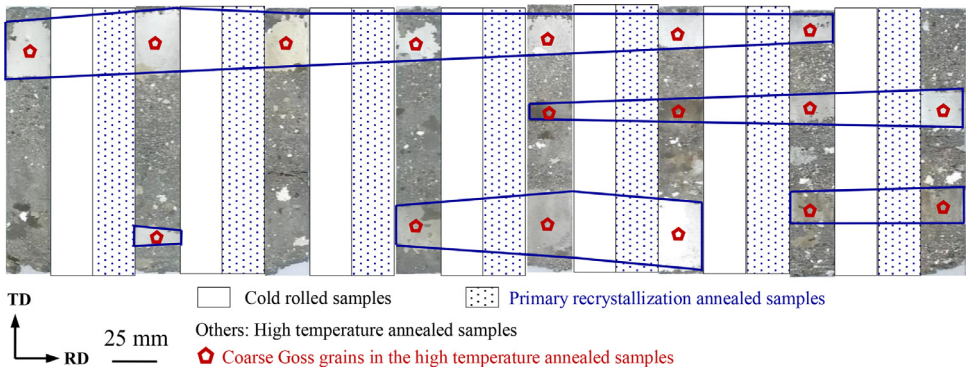

Fig. 5. RD-position resolved microstructures of the high temperature annealed samples in the tracking experiment of Route II. The blue frames outline the coarse Goss grains in the high temperature annealed samples as well as the cold rolled and primary recrystallization matrices associated with the secondary recrystallization regions.

cise Goss orientation and that having deviation angle of 15° was reduced to only 2.4% in the unconsumed matrix. As a result, the high-deviation-angle Goss grains might also undergo abnormal growth, competing with the low-deviation-angle Goss grains and leading to the weakened Goss texture and decreased magnetic inductions (Fig. 4(h)).

As shown in Fig. 9(a) and Fig. 9(b), the deviation angle distribution of Goss grains in the primary recrystallization matrix and the matrix prior to the onset of secondary recrystallization in Route I were similar with those in Route III despite of their distinct processing routes. Given this similar distribution and the results in Fig. 7 and Fig. 8, it could be inferred that the sharpness of final Goss texture might be mainly influenced by the environments after the onset of secondary recrystallization, i.e., the selection of growing Goss grains mainly undergo after the initiation of secondary recrystallization. Thus, the external heat flux direction [29] and other mechanisms might be resonsible for the abnormal growth of Goss grains in the early stage, while the combination of the frequencies

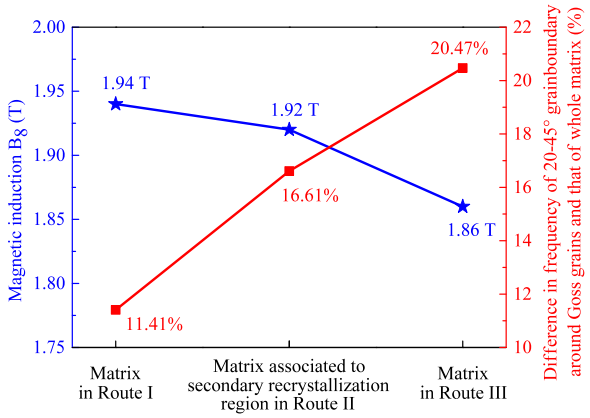

Fig. 6. Correlation between the magnetic induction B_8 value and the difference in the frequency of 20-45° grain boundaries. Here, the difference value was the frequency 20-45° grain boundaries around Goss grains minus that of whole primary recrystallization matrix.

of grains ($\leq$ 25 μm) having 20-45° disorientation with {110}<001> and the differences in the associated frequencies with precise Goss orientation and that having deviation angle of 15° might be used to evaluate the environments for the abnormal growth of low-deviation-angle Goss grains after the onset of secondary recrystallization. However, much effort still needs to be made to reveal the actual features determining the high mobility of the Goss grain boundaries instead of using the disorientation angle as the only boundary property.

It was reasonably inferred that the changes of the frequencies of certain grains in Fig. 7 were mainly related to the evolution of the γ-grains because they were in the majority in the primary recrystallization matrices (Fig. 3). For Route I, the area fraction of γ-grains was only decreased by 1.63% after the onset of secondary recrystallization (Fig. 9(c)) and the frequencies of low-deviation-angle (0-8°) Goss grains were only slightly decreased (Fig. 9(d)). This helped the retention of the favorable environments for the abnormal growth of Goss grains, see Fig. 7 and Fig. 8. By contrast, for Route III, the greatly-reduced area fraction (12.95%) of γ-grains (Fig. 9(c)) and increased frequencies of high-deviation-angle γ-grains (Fig. 9(d)) led to the decreased frequency of matrix grains ($\leq$ 25 μm) having 20-45° disorientation with {110}<001> and low difference in the associated frequencies with the precise Goss orientation and that having deviation angle of 15° after the onset of secondary recrystallization (Fig. 7 and Fig. 8).

3.3. *Effects of γ-grain colonies on the environments for abnormal growth of Goss grains*

The Route I and Route II (secondary recrystallization region) provided favorable environments for the abnormal growth of low-deviation-angle Goss grains even after the onset of secondary recrystallization. In order to reveal the underlying mechanisms, the micro-texture characteristics of various primary recrystallization matrices were investigated, see Fig. 10. In the primary recrystallization matrix in Route I and that associated with the secondary recrystallization region in Route II, a large proportion of γ-grains (with <111>//ND orientations) appeared as colonies along the rolling direction (Fig. 10(a) and Fig. 10(b)), which was sim-

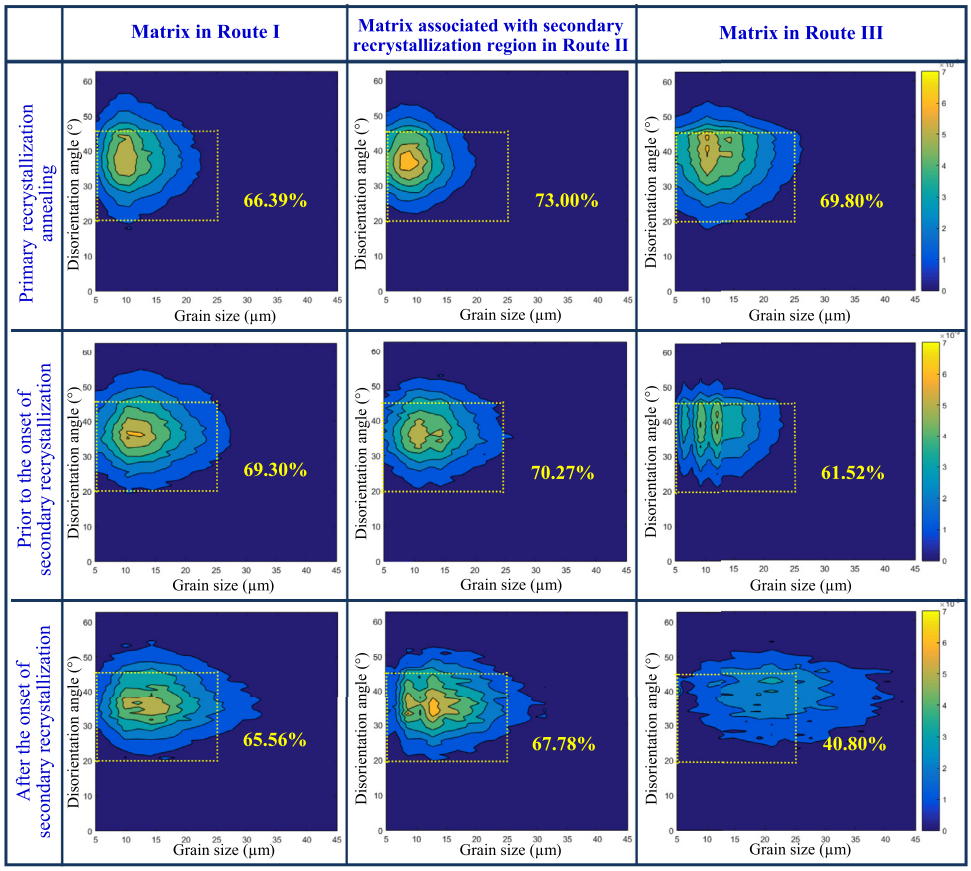

Fig. 7. Correlation between the grain size and the disorientation angle with precise Goss orientation ({110}<001>) of all the matrix grains in Route I, Route II-secondary recrystallization region and Route III.

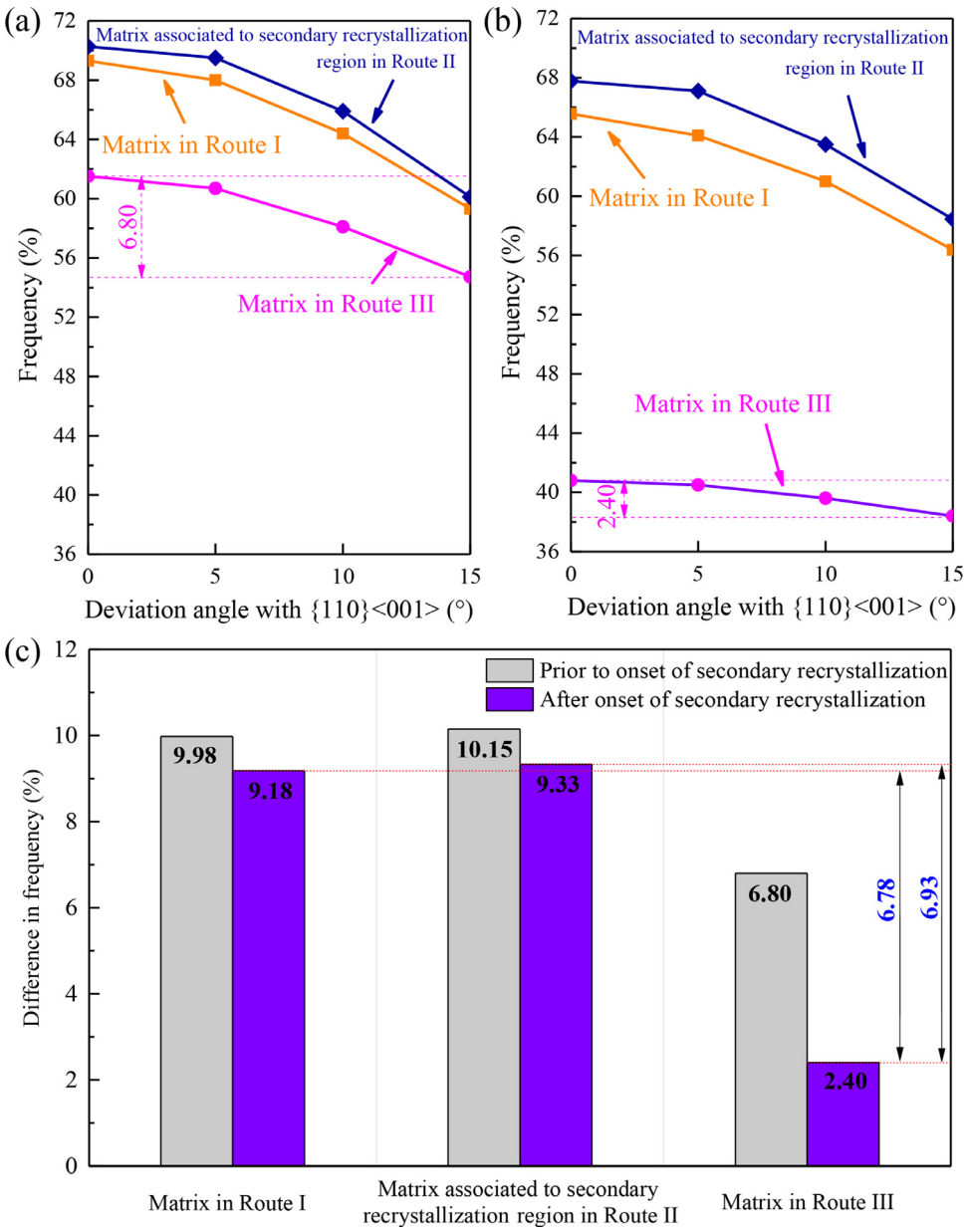

Fig. 8. The frequency of matrix grains (≤25μm) presenting 20-45° disorientation with the Goss orientation having various deviation angles in (a) the matrix prior to the onset of secondary recrystallization and (b) the unconsumed matrix after the onset of secondary recrystallization; (c) the frequency difference of the matrix grains (≤25μm) presenting 20-45° disorientation with precise Goss orientation and that having deviation angle of 15°.

ilar to those in stainless steels in case of one-stage cold rolling route [45,46]. The ODFs and grain boundary disorientation of the colonies were compared with those of entire matrices to verify the appearance of grain colonies. In the primary recrystallization matrix associated with the non-secondary recrystallization region in Route II, lots of large-sized (exceeding 1000 μm along the rolling direction and 400 μm along the transverse direction) λ-grain (with <001>//ND orientations) colonies appeared together with the γ-grain colonies (Fig. 10(c)). The bimodal distributions of the grain boundary disorientation in these three matrices also indicated the presence of many grain colonies, see Fig. 10(a), Fig. 10(b) and Fig. 10(c). By contrast, the matrix grains in the primary recrystallization matrix in Route III were nearly homogeneously-distributed. Thus, the grain boundary disorientation was quite similar to the Mackenzie distribution of random polycrystalline matrix [47,48].

As shown in Fig. 11, the primary recrystallization matrix in Route I, the primary recrystallization matrix associated with the secondary recrystallization region in Route II and the primary recrystallization matrix in Route III had similar average size as well as similar area fractions of γ-grains, λ-grains and Goss grains. The only difference was that the frequency of low-angle (0-15°) grain boundaries in the first two matrices was almost twice as many as that in Route III because of the presence of many grains colonies. As for the primary recrystallization matrix associated with the non-secondary recrystallization region in Route II, the area fraction of λ-grains was almost equivalent to that of γ-grains and the frequency of 0-15° grain boundaries was as high as 22.4% due to the presence of large-sized λ-grain colonies and γ-grain colonies. These micro-texture characteristics provided distinct environments for the abnormal growth of Goss grains.

According to Fig. 9(c), the reduced area fraction of γ-grains was mainly related to other matrix grains due to the limited change of the area fraction of Goss grains. Given that only the γ-grains on the colony edge were in contact with other matrix grains, the pres-

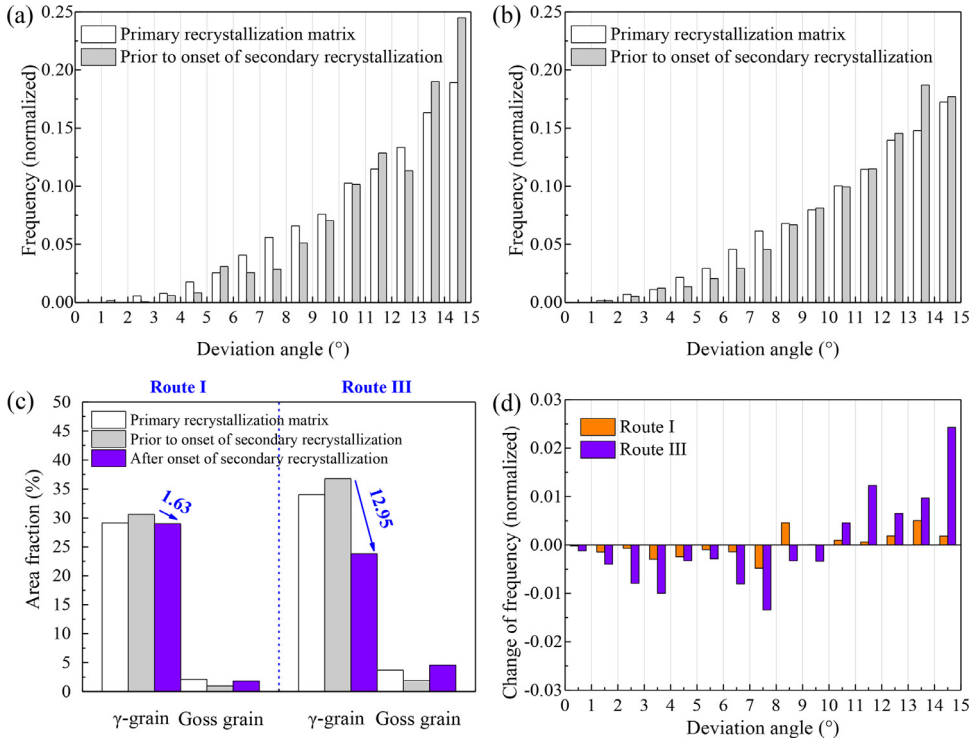

Fig. 9. Distribution of deviation angle of Goss grains in the primary recrystallization matrix and the matrix prior to the onset of secondary recrystallization in (a) Route I and (b) Route III; (c) area fraction evolution of γ-grains (deviation angle $\leq$15°) and Goss grains (deviation angle $\leq$15°) in Route I and Route III; (d) the frequency change of γ-grains in the matrix prior to and after the onset of secondary recrystallization.

ence of colonies might reduce the probability of γ-grains being consumed by other grains and those γ-grains within the colonies might survive due to the orientation pinning [49-51]. As a result, the presence of many γ-grain colonies led to the retention of relatively high area fraction of γ-grains even after the onset of secondary recrystallization, maintaining the desired environments for the abnormal growth of Goss grains. By contrast, the matrix grains in the primary recrystallization matrix in Route III were nearly randomly-distributed, suggesting that most γ-grains were in contact with other grains. This provided more opportunities for other grains to consume the γ-grains (Fig. 9(c)). As a result, the abnormal growth of high-deviation-angle Goss grains might be also facilitated after the onset of the secondary recrystallization, leading to the relatively weak final Goss texture.

In order to verify these inferences, three kinds of microstructures were generated (Fig. 12). The sizes of all the grains were assumed to be the same and the fraction of grains ($\leq$ 25μm) having 20-45° disorientation with {110}<001> were chosen as 60% (blue grains) according to Fig. 7. In the matrix with one grain colony (Fig. 12(a)), only 22.9% grains (with red dots) were on the colony edge. With increasing number of grain colonies, more grains were in contact with other matrix grains, see (Fig. 12(b)). In case of randomly-distributed grains (Fig. 12(c)), all the blue grains were in contact with other matrix grains and the length ratio of the blue grain/other grain boundaries versus blue grain/blue grain boundaries was as high as 71.4%, significantly increasing the probability of the γ-grains being consumed by other grains.

3.4. Detrimental effects of λ-grain colonies on secondary recrystallization

It is difficult for Goss grains to consume the λ-grains during high temperature annealing and thus the λ-grains may still exist even when the temperature is increased to a relatively high level [34]. Unfortunately, the λ-grains are readily retained along the processing route due to their low stored energy during rolling deformation [52-54]. As shown in Fig. 11(b), although the cold rolling reduction was up to ~88%, the area fraction of λ-grains was still as high as 14.7% and 16.6% in the primary recrystallization matrix in Route I and that associated with the secondary recrystallization region in Route II, respectively. However, the well-developed secondary recrystallization microstructures and sharp final Goss textures (Fig. 4) indicated that this kind of low-area-fraction and small-sized λ-grain colonies could not completely prevent the abnormal growth of Goss grains.

By contrast, the area fraction of λ-grains in the primary recrystallization matrix associated with the non-secondary recrystallization regions in Route II was as high as 21.6% and most λ-grains appeared as large-sized colonies, see Fig. 10(c) and Fig. 11(b). Given that most Goss grains were embodied in the γ-grain colonies (Fig. 13(a)), some Goss grains might still have suitable environments for abnormal growth in the early stage of high temperature annealing. However, the large-sized λ-grain colonies might block the further growth of these Goss grains. As shown in Fig. 13(b), an abnormally growing Goss grain was surrounded by the λ-grain colonies and its further growth would be restricted. With increasing annealing time, non-Goss grains might also grow abnormally, however, the sizes of these grains undergoing abnormal growth were still quite limited even after annealing at 1000°C for 45 minutes and 60 minutes, see Fig. 13(c) and Fig. 13(d). It seemed that most grains were subjected to normal growth, resulting in the non-secondary recrystallization regions composed of equiaxed grains with various orientations and low magnetic induction B_8 value in Fig. 4(e) and Fig. 4(f).

3.5. Formation of grain colonies in primary recrystallization matrix

As shown in Fig. 4, Fig. 7, Fig. 8 and Fig. 10, the presence of grain colonies in primary recrystallization matrix exerted important influences on the high temperature annealed microstructures

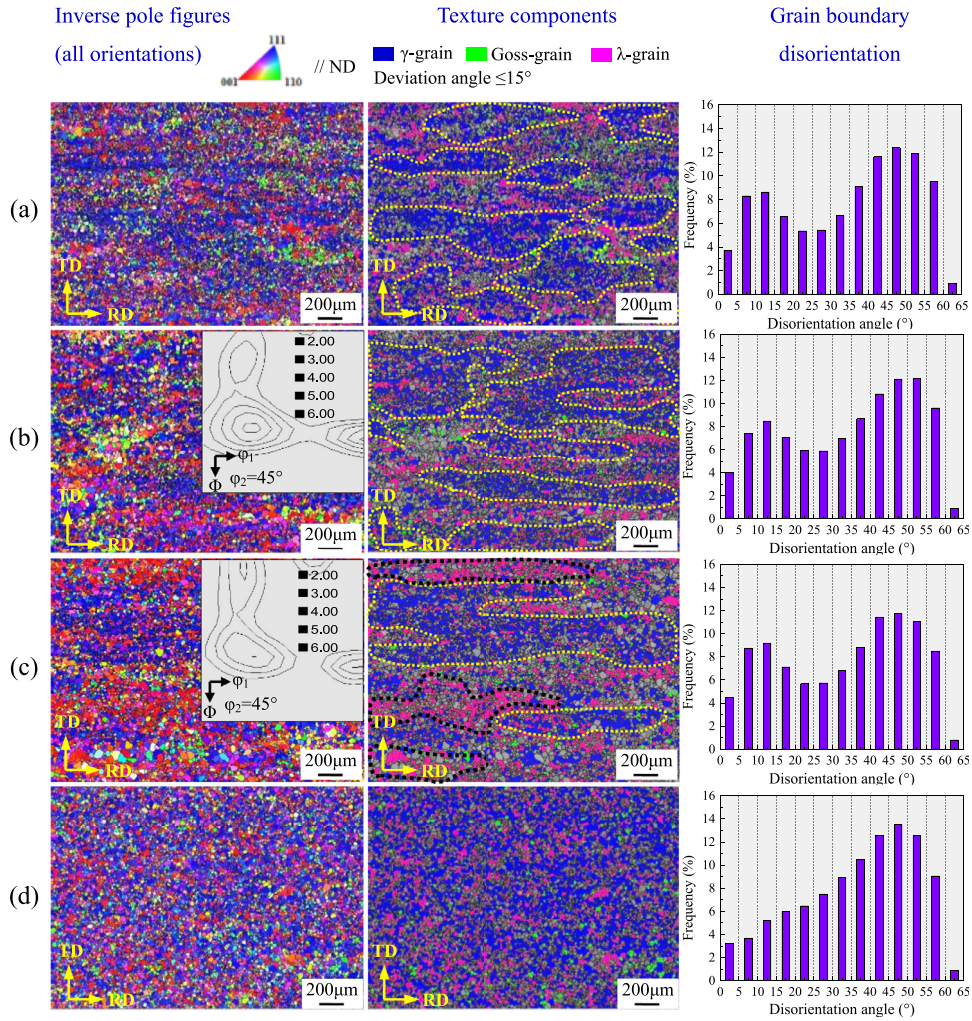

Fig. 10. ND IPF maps, the distribution of grains with selected orientations and the grain boundary disorientation in (a) the primary recrystallization matrix in Route I, (b) the primary recrystallization matrix associated with the secondary recrystallization region in the tracking experiment of Route II, (c) the primary recrystallization matrix associated with the non-secondary recrystallization region in the tracking experiment of Route II and (d) the primary recrystallization matrix in Route III.

and final Goss textures. In order to reveal the mechanisms for the formation of grain colonies, the microstructure and texture evolution during the processing route was investigated. For Route I, the fine solidification microstructure led to a relatively fine and homogeneous normalized microstructure (Fig. 14(a)). After severe cold rolling (88.8%), the initial fine and equiaxed grains were greatly extended along the rolling direction and dense deformation substructures appeared in almost all the deformed grains (Fig. 14(b)). The associated texture was characterized by a medium α-fiber texture and a strong {111}<110> component along γ-fiber texture. During primary recrystallization annealing, the preferential nucleation of {111}<112> grains within extended {111}<110> deformed grains [55] led to the formation of elongated γ-grain colonies.

For Route II, the dynamic recrystallization might occur during hot rolling due to the relatively high reduction (36.1%). However, the coarse solidification microstructure still led to an inhomogeneous normalized microstructure in which some regions had relatively fine microstructures with low proportion of λ-grains (Fig. 14(c)). After cold rolling (88.3%), the associated microstructure and texture were quite similar to those in Route I, see Fig. 14(b) and Fig. 14(d). Then, lots of large-sized γ-grain colonies were generated in the primary recrystallization matrix associated with the secondary recrystallization regions. By contrast, some regions of the normalized sheet were comprised of high-proportion coarse λ-grains (Fig. 14(e)). Many large λ-grains with little sign of deformation substructures were retained even after severe cold rolling (Fig. 14(f)). The corresponding cold rolled texture was composed of weak {111}<110> texture, medium α-fiber texture and strong {001}<110> texture at the λ-fiber. As a result, the high-proportion large-sized λ-grain colonies were also formed together with the γ-grain colonies in the primary recrystallization matrix associated with the non-secondary recrystallization regions (Fig. 14(f)).

For Route III, the first cold rolling and intermediate annealing led to a fine and homogeneous microstructure with low-proportion λ-grains, see Fig. 14(g). Because of the moderate reduction (~66.3%) of second cold rolling, the initial equiaxed ferrite grains were only slightly elongated and a weak γ-fiber texture was formed (Fig. 14(h)). This resulted in the homogeneously-distributed grains with various orientations in the primary recrystallization matrix.

These results suggested that the formation of grain colonies was mainly related to the initial solidification microstructure, the processing routes as well as the deformation and recrystallization features of γ-grains and λ-grains. This is also of important guiding significance for manufacturing the grain-oriented electrical steels by strip casting route. Given the lack of heavy-reduction hot rolling in this particular route, it is critical to reduce the proportion of coarse λ-grains by controlling the solidification during strip casting.

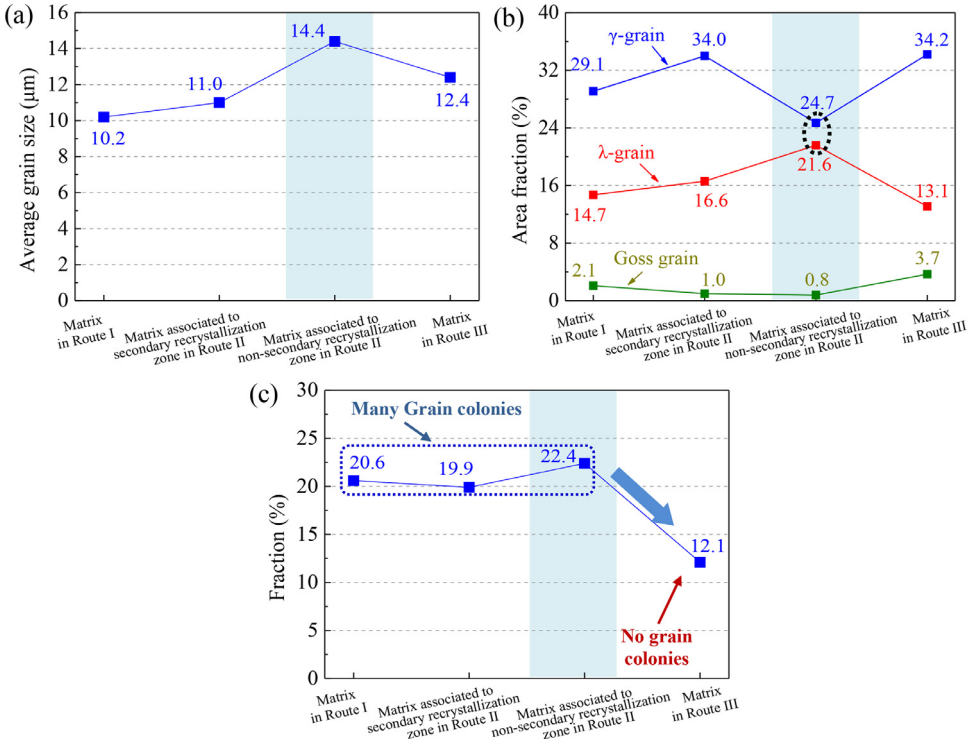

Fig. 11. (a) Average grain size, (b) area fraction of the grains with selected orientations and (c) fraction of low-angle (0-15°) grain boundaries in the primary recrystallization matrices from different routes.

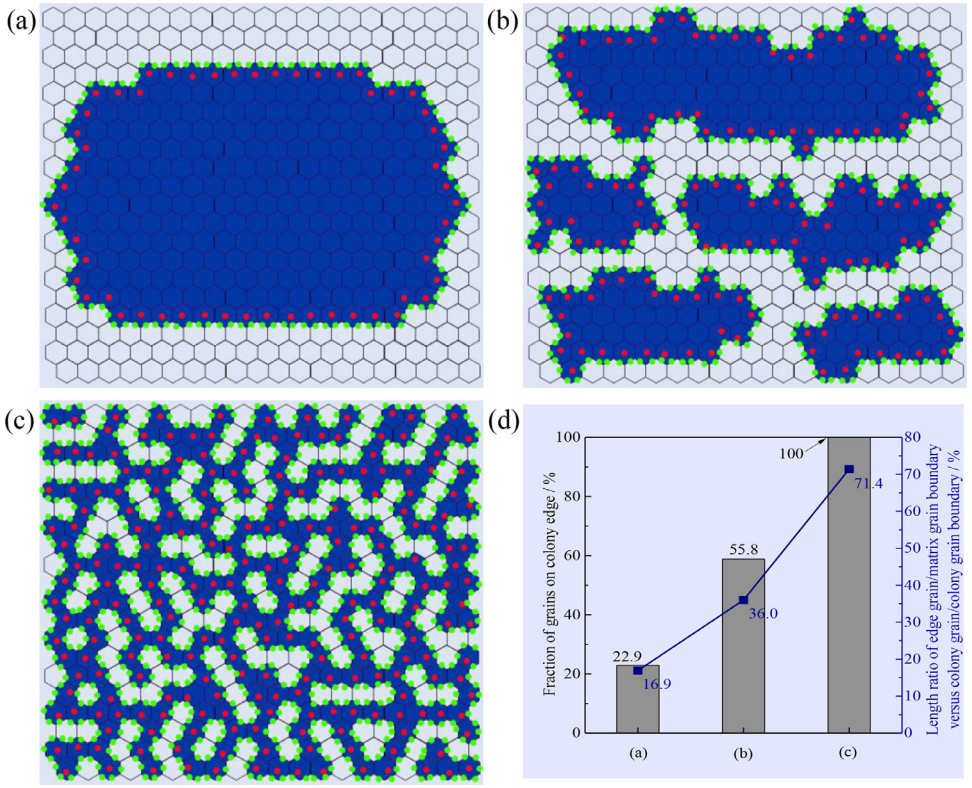

Fig. 12. Schematic diagram showing the primary recrystallization matrix with (a) one grain colony composed of the grains (≤ 25μm) having 20-45° disorientation with {110}<001>, (b) five grain colonies and (c) randomly-distributed grains; (d) correlation between the grain distribution and the fractions of grains on colony edges and length ratio of edge grain/other matrix grain boundaries versus colony grain/colony grain boundaries. Blue grains: the matrix grains (≤ 25μm) having 20-45° disorientation with {110}<001>; Red dots: the blue grains in contact with other matrix grains; Greet dots: the blue grain/other matrix grain boundaries.

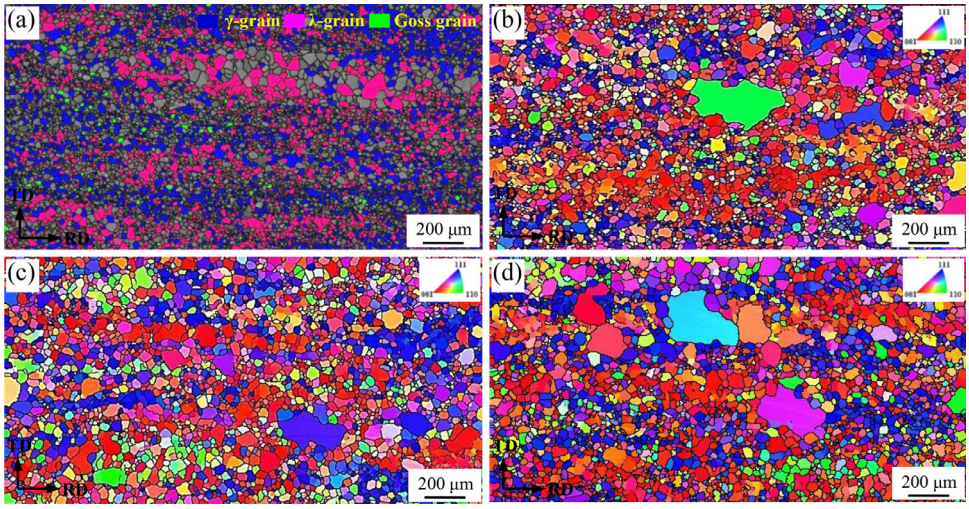

Fig. 13. (a) Distribution of the grains with selected orientations (deviation angle ≤15°) in primary recrystallization matrix, (b) ND-IPF of the matrix annealed at 1000°C for (b) 30 minutes, (c) 45 minutes and (d) 60 minutes associated with the non-secondary recrystallization regions in the tracking experiment of Route II.

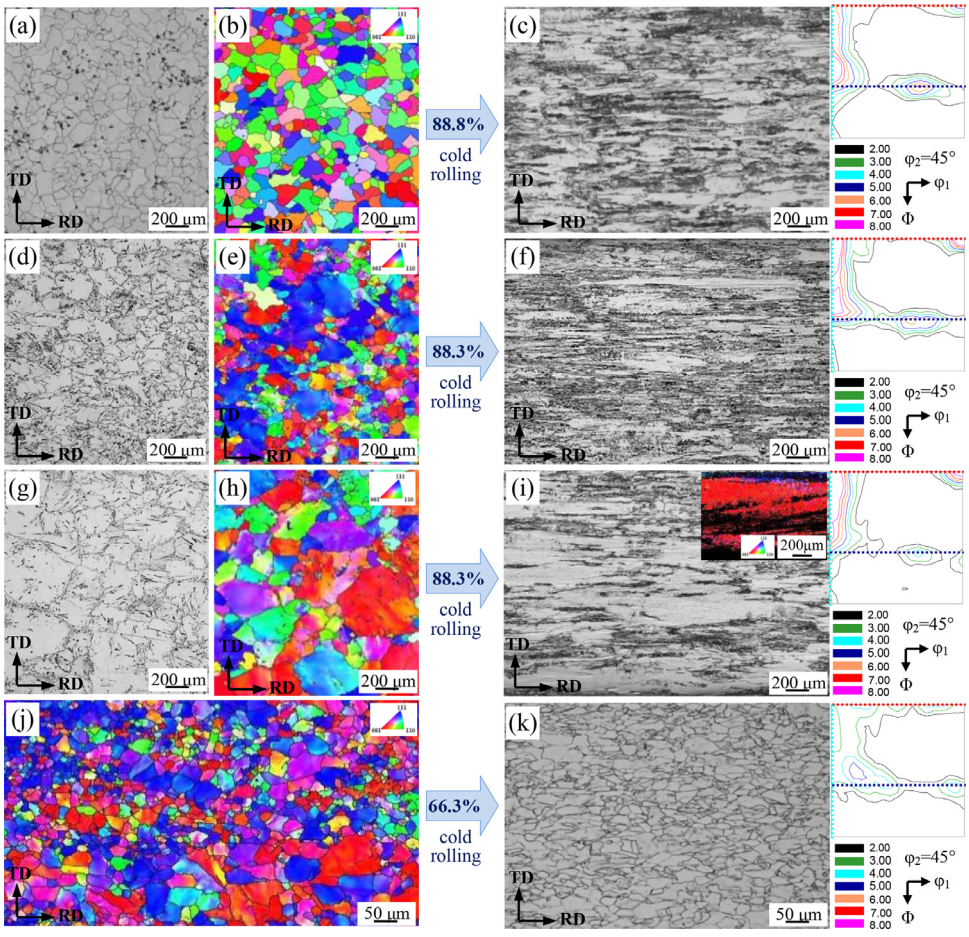

Fig. 14. (a) Microstructure and (b) ND-IPF of the normalized sheet, (c) microstructure and texture (φ_2=45° section) of the cold rolled sheet in Route I; (d)(g) microstructures and (e)(h) ND-IPFs of the normalized sheet, (f)(i) microstructures and textures (φ_2=45° section) of the corresponding cold rolled sheets in Route II; (j) ND-IPF of the intermediate annealed sheet and (k) microstructure and texture (φ_2=45° section) of the second cold rolled sheet in Route III.

4. Conclusions

The present study investigated the role of grain colony in primary recrystallization matrix on the secondary recrystallization in grain-oriented electrical steels via an original tracking experiment. The main conclusions are summarized as follows.

(1) We observed that the presence of γ-grain colonies facilitated the retention of matrix grains ($\leq$ 25 μm) having 20-45° disorientation with {110}<001> and relatively large difference in the associated frequencies with the precise Goss orientation and that having deviation angle of 15° even after the onset of secondary recrystallization. This promoted the

abnormal growth of low-deviation-angle Goss grains and led to the sharp final Goss texture. By contrast, in case of the randomly-distributed γ-grains in the primary recrystallization matrix, the high-deviation-angle Goss grains might be also subjected to abnormal growth after the initiation of secondary recrystallization due to the limited difference in the associated frequencies with the precise Goss orientation and that having deviation angle of 15°. The presence of a great number of large-sized λ-grain colonies in primary recrystallization matrix deteriorated the environments for secondary recrystallization and thus most grains were only subjected to normal grain growth.

(2) The formation of grain colonies was mainly related to the initial solidification microstructure, processing route as well as deformation and recrystallization features of γ-grains and λ-grains. In case of coarse solidification microstructure with high proportion of λ-grains, the employment of two-stage cold rolling route resulted in randomly-distributed grains with various orientations, eliminating the large-sized λ-grain colonies generated in one-stage cold rolling route. These findings provided an explanation for the effects of processing route and primary recrystallization texture on the abnormal growth of Goss grains, especially after the initiation of secondary recrystallization, with the presence of grain colonies.

Declaration of Competing Interest

The authors declare that they have no known competing financial interests or personal relationships that could have appeared to influence the work reported in this paper.

Acknowledgements

This work was supported by the National Key Research and Development Program of China (2016YFB0300305); the National Natural Science Foundation of China (grant numbers 51574078, 51774081 and 51804073); the China Postdoctoral Science Foundation (grant numbers 2016T90228, 2018M630296 and 2020T130082); the Fundamental Research Funds for the Central Universities (grant numbers N170703007 and N180712004) and the LiaoNing Revitalization Talents Program (XLYC1907056). The authors are deeply indebted to the three anonymous reviewers for their valuable comments and suggestions that contributed to clarify several interpretations presented in this manuscript.

References

[1] M. Matsuo, Texture Control in the Production of Grain Oriented Silicon Steels, ISIJ Int 29 (10) (1989) 809–827.
[2] C.S He, Y.D. Zhang, Y.N. Wang, X. Zhao, L. Zuo, C. Esling, Texture and microstructure development in cold-rolled interstitial free (IF) steel sheet during electric field annealing, Scripta Mater 48 (6) (2003) 737–742.
[3] Y.D. Zhang, C. Esling, J.S. Lecomte, C.S. He, X. Zhao, L. Zuo, Grain boundary characteristics and texture formation in a medium carbon steel during its austenitic decomposition in a high magnetic field, Acta Mater 53 (19) (2005) 5213–5221.
[4] J. Humphreys, G.S. Rohrer, A. Rollett, Recrystallization and Related Annealing Phenomena, Elsevier, 2017 third ed..
[5] Q. Fu, Y.H. Sha, F. Zhang, C. Esling, L. Zuo, Correlative effect of critical parameters for eta recrystallization texture development in rolled Fe81Ga19 sheet: Modeling and experiment, Acta Mater 167 (2019) 167180.
[6] A.L. Etter, T. Baudin, R. Penelle, Influence of the Goss grain environment during secondary recrystallisation of conventional grain oriented Fe-3%Si steels, Scripta Mater 47 (11) (2002) 725–730.
[7] J.Y. Park, K.S. Han, J.S. Woo, S.K. Chang, N. Rajmohan, J.A. Szpunar, Influence of primary annealing condition on texture development in grain oriented electrical steels, Acta Mater 50 (7) (2002) 1825–1834.
[8] C.G. Dunn, Cold Working of Metals, ASM, Cleveland, 1949.
[9] C.G. Dunn, Secondary recrystallization textures and their origin in cold-rolled single crystals of silicon iron, Acta Metall 1 (2) (1953) 163–175.
[10] D. Dorner, S. Zaefferer, D. Raabe, Retention of the Goss orientation between microbands during cold rolling of an Fe3%Si single crystal, Acta Mater 55 (2007) 2519–2530.
[11] Y. Ushigami, M. Mizokami, M. Fujikura, T. Kubota, H. Fujii, K. Murakami, Recent development of low-loss grain-oriented electrical steel, J. Magn. Magn. Mater. 254 (2003) 307–314.
[12] H.T. Liu, S.J. Yao, Y. Sun, F. Gao, H.Y. Song, G.H. Liu, L. Li, D.W. Geng, Z.Y. Liu, G.D. Wang, Evolution of microstructure, texture and inhibitor along the processing route for grain-oriented electrical steels using strip casting, Mater. Charact. 106 (2015) 273–282.
[13] M. Hillert, On the theory of normal and abnormal grain growth, Acta Metall 13 (1965) 227–238.
[14] J.E. Burke, D. Turnbull, Recrystallization and grain growth, Prog. Met. Phys. 3 (1952) 220–292.
[15] R. Shimizu, J. Harase, Coincidence grain boundary and texture evolution in Fe-3%Si, Acta Metall 37 (4) (1989) 1241–1249.
[16] J. Harase, R. Shimizu, Coincidence grain boundary and (110)[001]secondary recrystallization in Fe-3% Si, Acta Metall. Mater. 40 (1992) 1101–1111.
[17] Y. Yoshitomi, Y. Ushigami, J. Harase, T. Nakayama, H. Masui, N. Takahashi, Coincidence grain boundary and role of primary recrystallized grain growth on secondary recrystallization texture evolution in Fe-3%Si alloy, Acta Metall. Mater. 42 (1994) 2593–2602.
[18] Y. Hayakawa, J.A. Szpunar, A new model of Goss texture development during secondary recrystallization of electrical steel, Acta Mater 45 (11) (1997) 4713–4720.
[19] Y. Hayakawa, J.A. Szpunar, The role of grain boundary character distribution in secondary recrystallization of electrical steels, Acta Mater 45 (1997) 1285–1295.
[20] Y. Hayakawa, M. Muraki, J.A. Szpunar, The changes of grain boundary character distribution during the secondary recrystallization of electrical steel, Acta Mater 46 (3) (1998) 1063–1073.
[21] A. Morawiec, Grain misorientations in theories of abnormal grain growth in silicon steel, Scripta Mater 43 (2000) 275–278.
[22] A. Morawiec, On abnormal growth of Goss grains in grain-oriented silicon steel, Scripta Mater 64 (2011) 466–469.
[23] K.J. Ko, J.T. Park, J.K. Kim, N.M. Hwang, Morphological evidence that Goss abnormally growing grains grow by triple junction wetting during secondary recrystallization of Fe-3% Si steel, Scripta Mater 59 (2008) 764–767.
[24] K.J. Ko, P.R. Cha, D. Srolovitz, N.M. Hwang, Abnormal grain growth induced by sub-boundary-enhanced solid-state wetting: analysis by phase-field model simulation, Acta Mater 57 (2009) 838–845.
[25] H.K. Park, S.D. Kim, S.C. Park, J.T. Park, N.M. Hwang, Sub-boundaries in abnormally growing Goss grains in Fe–3% Si steel, Scripta Mater 62 (6) (2010) 376–378.
[26] J.K. Kim, J.S. Woo, S.K. Chang, Influence of annealing before cold rolling on the evolution of sharp Goss texture in Fe-3%Si alloy, J. Magn. Magn. Mater. 215 (2000) 162–164.
[27] S.K. Chang, Texture change from primary to secondary recrystallization by hot band normalizing in grain-oriented silicon steels, Mater. Sci. Eng. A. 452-453 (2007) 93–98.
[28] S.F. Castro, J. Gallego, F.J.G. Landgraf, H.-J. Kestenbach, Orientation dependence of stored energy of cold work in semi-processed electrical steels after temper rolling, Mater. Sci. Eng. A. 427 (2006) 301–305.
[29] S. Birosca, A. Nadoum, D. Hawezy, F. Robinson, W. Kockelmann, Mechanistic approach of Goss abnormal grain growth in electrical steel: Theory and argument, Acta Mater 185 (2020) 370–381.
[30] T. Kumano, T. Haratani, Y. Ushigami, The improvement of primary texture for sharp Goss orientation of grain oriented silicon steel, ISIJ Int 43 (5) (2003) 736–745.
[31] F. Fang, M.F. Lan, X. Lu, Y.X. Zhang, Y. Wang, G. Yuan, G.M. Cao, Y.B. Xu, R.D.K. Misra, G.D. Wang, The impact of niobium on the microstructure, texture and magnetic properties of strip-cast grain oriented silicon steel, J. Magn. Magn. Mater. 442 (2017) 1–7.
[32] Y. Gao, G. Xu, X. Guo, G. Li, Y. Wang, Primary recrystallization characteristics and magnetic properties improvement of high permeability grain-oriented silicon steel by trace Cr addition, J. Magn. Magn. Mater. 507 (2020) 166849.
[33] S. Mishra, C. Därmann, K. Lücke, New information on texture development in regular and high-permeability grain-oriented electrical steels, Metall. Trans. A. 17A (1986) 1301–1312.
[34] J.Y. Park, K.S. Han, J.S. Woo, S.K. Chang, N. Rajmohan, J.A. Szpunar, Influence of primary annealing condition on texture development in grain oriented electrical steels, Acta Mater 50 (2002) 1825–1834.
[35] H.Y. Song, H.T. Liu, Y.P. Wang, G.D. Wang, Secondary recrystallization behavior in a twin-roll cast grain-oriented electrical steel, J. Magn. Magn. Mater. 428 (2017) 325–332.
[36] A. Bastos, S. Zaefferer, D. Raabe, C. Schuh, Characterization of the microstructure and texture of nanostructured electrodeposited NiCo using electron backscatter diffraction (EBSD), Acta Mater 54 (2006) 2451–2462.
[37] V. Randle, G.S. Rohrer, Y. Hu, Five-parameter grain boundary analysis of a titanium alloy before and after low-temperature annealing, Scripta Mater 58 (3) (2008) 183–186.
[38] M. Mehdi, Y. He, E.J. Hilinski, L.A.I. Kestens, A. Edrisy, The evolution of cube ({001}<100>) texture in non-oriented electrical steel, Acta Mater 185 (2020) 540–554.

[39] H.T. Liu, Z.Y. Liu, Y.Q. Qiu, G.M. Cao, C.G. Li, G.D. Wang, Characterization of the solidification structure and texture development of ferritic stainless steel produced by twin-roll strip casting, Mater. Charact. 60 (2009) 79–82.
[40] H. Liu, Z. Liu, C. Li, G. Cao, G. Wang, Solidification structure and crystallographic texture of strip casting 3 wt.% Si non-oriented silicon steel, Mater. Charact. 62 (2011) 463–468.
[41] H.J. Bunge, Texture Analysis in Materials Science: Mathematical Methods, Butterworths, London, 1982.
[42] O. Engler, V. Randle, Introduction to texture anaylysis: macrotexture, microtexture and orientation mapping, CRC Press, 2010 second edition.
[43] Z. Xia, Y. Kang, Q. Wang, Developments in the production of grain-oriented electrical steel, J. Magn. Magn. Mater. 320 (2008) 3229–3233.
[44] D. Dorner, S. Zaefferer, L. Lahn, D. Raabe, Overview of microstructure and microtexture development in grain-oriented electrical steel, J. Magn. Magn. Mater. 304 (2006) 183–186.
[45] F. Gao, Z. Liu, H. Liu, G. Wang, Texture evolution and formability under different hot rolling conditions in ultra purified 17%Cr ferritic stainless steels, Mater. Charact. 75 (2013) 93–100.
[46] D.G. Rodrigues, C.M. Alcâmtara, T.R. Oliveira, B.M. Gonzalez, The effect of grain size and initial texture on microstructure, texture, and formability of Nb stabilized ferritic stainless steel manufactured by two-step cold rolling, J. Mater. Res. Technol. 8 (2019) 4151–4162.
[47] J.K. Mackenzie, Second paper on statistics associated with the random disorientation of cubes, Biometrika 45 (1958) 229–240.
[48] J.K. Mason, C.A. Schuh, The generalized Mackenzie distribution: Disorientation angle distributions for arbitrary textures, Acta Mater 57 (2009) 4186–4197.
[49] R.D. Doherty, D.A. Hughes, F.J. Humphreys, J.J. Jonas, D. Jull Jensen, M.E. Kassner, W.E. King, T.R. McNelley, H.J. McQueen, A.D. Rollett, Current issues in recrystallization: a review, Mater. Sci. Eng. A. 238 (1997) 219–274.
[50] O. Engler, On the influence of orientation pinning on growth selection of recrystallization, Acta Mater 46 (5) (1998) 1555–1568.
[51] R.D. Doherty, L.C. Chen, I. Samajdar, Cube recrystallization texture-experimental results and modeling, Mater. Sci. Eng. A. 257 (1) (1998) 18–36.
[52] N. Tsuji, K. Tsuzaki, T. Maki, Effect of Initial Orientation on the Cold Rolling Behavior of Solidified Columnar Crystals in a 19% Cr Ferritic Stainless Steel, ISIJ Int 32 (12) (1992) 1319–1328.
[53] N. Tsuji, K. Tsuzaki, T. Maki, Effect of Initial Orientation on the Recrystallization Behavior of Solidified Columnar Crystals in a 19% Cr Ferritic Stainless Steel, ISIJ Int 33 (7) (1993) 783–792.
[54] H.Y. Song, H.T. Liu, J.J. Jonas, G.D. Wang, Effect of primary recrystallization microstructure on abnormal growth of Goss grains in a twin-roll cast grain-oriented electrical steel, Mater. Design 131 (2017) 167–176.
[55] J.T. Park, J.A. Szpunar, Evolution of recrystallization texture in nonoriented electrical steels, Acta Mater 51 (2003) 3037–3051.